Energetic outer radiation-belt electron precipitation during recurrent solar activity

Mark A. Clilverd

Physical Sciences Division, British Antarctic Survey (NERC), Cambridge, United Kingdom

Craig J. Rodger

Department of Physics, University of Otago, Dunedin, New Zealand

Tracy Moffat-Griffin

Physical Sciences Division, British Antarctic Survey (NERC), Cambridge, United Kingdom

Emma Spanswick

Dept. of Physics and Astronomy, University of Calgary, Calgary, Canada

Paul Breen

Physical Sciences Division, British Antarctic Survey (NERC), Cambridge, United Kingdom

Frederick W. Menk

School of Mathematical and Physical Sciences, University of Newcastle, Callaghan, Australia.

Russell S. Grew

School of Mathematical and Physical Sciences, University of Newcastle, Callaghan, Australia.

Kanji Hayashi

Department of Earth and Planetary Physics, University of Tokyo, Japan.

Ian R. Mann

Department of Physics, University of Alberta, Edmonton, Canada.

Abstract. Transmissions from three U.S. VLF transmitters were received at Churchill, Canada, during an event study in May-November, 2007. This period spans four

cycles of recurrent geomagnetic activity spaced ~27 days apart, with daily sum Kp reaching ~30 at the peaks of the disturbances. The difference in the amplitude of the signals received between daytime and nighttime varied systematically with geomagnetic activity, and was used here as a proxy for ionization changes caused by energetic electron precipitation. For the most intense of the recurrent geomagnetic storms there was evidence of electron precipitation from $3<L<7$ for 10-15 days after the peak of the disturbance as measured by ΣKp and Dst. This was consistent with the time variation of the fluxes of POES >300 keV and ~1 MeV trapped electrons, and consistent with the daily average ULF Pc1-2 power from Lucky Lake, Canada, (L=3.9) which was elevated during the ~1 MeV electron precipitation period. Suggesting that Pc1-2 waves may play a role in outer radiation belt loss processes during this interval. We show that the >300 keV trapped electron flux from POES is a reasonable proxy for electron precipitation during recurrent high speed solar wind streams, although it did not describe all of the variability that occurred. While energetic electron precipitation can be described through a proxy such as Kp or Dst, careful incorporation of time delays for different electron energies must be included. Dst was found to be the most accurate proxy for electron precipitation during the weak recurrent activity period studied.

1. Introduction

The influence of radiation belt processes on the Earth's atmosphere is currently a topic of intense debate. As energetic particles precipitate into the upper atmosphere they enhance in-situ ionization rates [Siskind, 2000], and this results in chemical composition changes as odd nitrogen (NO_x) and odd hydrogen (HO_x) compounds are created [Solomon et al., 1982]. HO_x and NO_x take part in the catalytic destruction of ozone and hence change the radiative balance of the atmosphere [Brasseur and Solomon, 2005]. Although HO_x is a short-lived species and only acts on ozone in-situ, NO_x is long-lived (lifetime of days to months) in the absence of photolysis, and can therefore be transported horizontally and vertically during its lifetime. This is particularly true in the dark polar wintertime, and in the presence of the polar vortex [Randall et al., 2005; Manney et al., 2005]. As such, the products of energetic particle precipitation processes can have a long-lived and distributed effect on the chemistry and radiative balance of the atmosphere [Rozanov et al., 2005; Seppälä et al., 2009].

Energetic proton precipitation occurring during solar proton events (SPEs) is a well-known influence on the atmosphere [Seppälä et al., 2004]. During some intense solar storms solar protons in the energy range 1 to >100 MeV enter the atmosphere in the polar regions, having been guided by the geomagnetic field [Rodger et al., 2006]. Proton flux measurements made from geostationary satellites (i.e., GOES) have been shown to be good proxies for the flux and energy spectrum of protons entering the atmosphere [Verronen et al., 2005; Clilverd et al., 2005, 2006a]. The highest energy

protons can occasionally penetrate as low as the ground, although typically the lowest altitude influenced is 40-50 km [Seppälä et al., 2008]. The lower energy protons scatter in the atmosphere at much higher altitudes (~120 km for 1 MeV protons) but are still capable of ionizing the atmospheric constituents [Turunen et al., 2009].

However, while SPEs are intense, they are relatively infrequent, and typically only last for a few days [Shea and Smart, 1990; Richardson et al., 2000]. When they do occur, SPEs are more frequent during the 11-year solar cycle maximum than at solar minimum [Borovsky and Denton, 2006]. In contrast, energetic electron precipitation driven by radiation belt processes is less well understood in terms of measurements of the flux and location of electrons entering the atmosphere. Further, there is considerable uncertainty as to the energy spectra of the electron precipitation, with multiple radiation belt processes taking place, such as acceleration and loss by several different VLF wave-particle interaction processes [Imhof et al., 1992; Blake et al., 1996; Millan et al., 2002; Horne, 2002], and radial transport by ULF waves [Fei et al., 2006 and references therein]. Energy diffusion due to electron gyroresonance with chorus, plasmaspheric hiss, and electromagnetic ion-cyclotron waves (EMIC) have been shown to be key mechanisms for generating relativistic electrons in the region outside of the plasmasphere during geomagnetic storms [e.g., Summers et al., 2007, and references therein]. Recent progress in the understanding of the acceleration of energetic electrons in the outer radiation belt due to nonlinear wave-particle interactions by the relativistic second-order resonance condition for whistler-mode waves is described in Omura et al. [2008]. Gyroresonant pitch-angle

scattering of electrons by chorus, plasmaspheric hiss, and EMIC waves can lead to significant precipitation into the atmosphere and net loss of energetic electrons from the outer radiation belt [e.g., Lorentzen et al., 2001; O'Brien et al., 2004; Thorne et al., 2005; Rodger et al., 2007, Rodger et al., 2008].

Recent results have shown that radiation belt acceleration processes are more significant during recurrent high speed solar wind stream storms (HSSWS) in comparison with those storms driven by coronal mass ejections (CMEs) [Hilmer et al., 2000; Miyoshi and Kataoka, 2005; Vassiliadis et al., 2007]. Radiation belt electron precipitation has been shown to be longer lasting during HSSWS than during CMEs [Longden et al., 2008]. HSSWS storms occur more frequently during the declining-minimum phase of the 11-year solar cycle [Borovsky and Denton, 2006]. Generally, radiation belt electron precipitation processes can be thought of as driving electrons into the atmosphere at mid- to polar latitudes, and with a peak occurrence frequency during the declining phase of the 11-year solar cycle. However the detailed time variability, energy spectrum, and flux have proved difficult to measure.

Satellite measurements of electron precipitation properties have been available for more than a solar cycle (e.g., SAMPEX, POES). However each satellite instrument has some limitations in either spatial resolution, or energy resolution, or suffers from low energy proton contamination, or has an inability to adequately resolve the drift/bounce loss-cone. These issues result in uncertainties as to the actual loss rates of electrons into the atmosphere when measured from satellites. For example, Rodger et al. [2010] analysed 10-years of POES data [Evans and Greer, 2004] to provide a

description of energetic electron precipitation with a comprehensive study of enhanced loss fluxes from the radiation belts, but with limited energy spectrum resolution.

Ground-based measurements of the lower ionosphere can help contextualise satellite measurements of electron precipitation. Obliquely propagating VLF radio waves can be used to monitor the changes in ionization rate caused by electron precipitation over a great circle path between a transmitter and a receiver. The AARDDVARK network [Clilverd et al., 2009] makes use of this property to determine the path-integrated effect of electron precipitation in many high-latitude locations around the world. The enhancement in ionization rate as a result of electron precipitation causes changes in the received phase and amplitude of the observed signals, which can be readily compared with the non-disturbed quiet-day behaviour.

In this study we analyse data from an AARDDVARK receiver located in Churchill, Canada, and concentrate on signals from three US transmitters (call signs NAA, NDK, NLK). The signals are used to determine the effects of electron precipitation into the atmosphere over the range $3<L<8$, i.e., where outer radiation belt processes occur. We study the period May-November 2007 which includes several recurrent (HSSWS) solar activity cycles, and analyse the Churchill AARDDVARK data in comparison with POES electron flux observations at >300 keV and >1 MeV. The radio-wave propagation effects observed are then described in terms of the effectiveness of recurrent solar activity in producing energetic electron precipitation into the atmosphere.

2. Experimental setup

Figure 1 shows the geomagnetic conditions during the May-November 2007 period that is studied in this paper. The solar wind speed, daily ΣKp, daily Dst, and daily GOES >2 MeV electron flux are plotted in separate panels, ordered from top to bottom. Each panel also shows a 7-day smoothed line (solid line) for each parameter. The solar wind speed ranged from 250 km/s to 700 km/s. After day 210 a HSSWS feature appeared which repeated four times, with a 27-day period. During this period the solar wind speeds consistently peaked at ~650 km/s, dropping to ~250 km/s 10-days after the peak. The ΣKp and Dst values followed a very similar pattern to the solar wind speed, with the highest geomagnetic disturbance occurring on the third recurrence of the HSSWS activity. Very similar patterns of behaviour can be seen in the GOES electron fluxes, where high solar wind and high geomagnetic activity were associated with high electron flux levels at geostationary orbit. The peak times of the 27-day recurrent activity in solar wind, geomagnetic activity, and high L=6.6 electron fluxes are indicted by the dot-dashed vertical lines. For clarity we have labeled the recurrent storm activity cycles 1, 2, 3, and 4. We note that during the May-November 2007 period studied here there were no occasions where elevated solar proton flux occurred which could potentially mask the effects of energetic electron precipitation into the high-latitude atmosphere.

To study the electron precipitation effects into the atmosphere during the May-November 2007 period this paper uses narrow band subionospheric very low frequency (VLF) data spanning 24-25 kHz received at Churchill, Canada (geographic 58º44’N, 93º49’W, L=7.6). The Churchill site is part of the Antarctic-Arctic

Radiation-belt Dynamic Deposition VLF Atmospheric Research Konsortia (AARDDVARK) network (Clilverd et al., [2009], for further information see the description of the array at www.physics.otago.ac.nz/space/AARDDVARK_homepage.htm). The transmitters studied have call-signs NAA (24.0 kHz, geographic 44º39'N, 67º17'W, L=2.9), NDK (25.2 kHz, geographic 46º22'N, 98º20'W, L=3.2), and NLK (24.8 kHz, , 48º12'N, 121º55'W, L=2.9). The effects of changing ionization conditions in the mesosphere, due to energetic particle precipitation, can be observed along the propagation path between a transmitter and a receiver. Subionospheric propagation is sensitive to ionization located below about 90 km altitude. The effect of increased ionization on the propagating signals can be seen as either an increase or decrease in signal amplitude or phase depending on the modal mixture of each signal observed [Barr et al., 2000, Clilverd et al., 2007].

Figure 2 shows the location of the Churchill radio wave receiver site (diamond), and the transmitter-receiver paths that are studied during the event period (NAA, NDK, and NLK transmitter locations are shown by the circles). The propagation paths span the range $3<L<8$, effectively integrating the subionospheric electron precipitation along the paths from the whole of the outer radiation belt. The three paths analysed are relatively short, the transmitters are very similar in frequency, and their geomagnetic latitudes are also very similar. As such, we combine the data from the three transmitters in order to confirm that large scale precipitation effects are occurring on all three paths at the same time.

In this study we also make use of particle measurements by the Space

Environment Monitor-2 instrument package onboard the POES spacecraft which are in Sun-synchronous orbits at ~800-850 km altitudes [Evans and Greer, 2004]. SEM-2 includes the Medium Energy Proton and Electron Detector (MEPED), in addition to the Total Energy Detector (TED). Together these instruments monitor electron fluxes from 50 eV up to 2700 keV. We make use of SEM-2 observations from up to 4 POES spacecraft. All POES data are available from http://poes.ngdc.noaa.gov/data/; while the full-resolution data have 2-s time resolution, we work with the 16-s resolution ASCII files. The 0º-pointing detectors are mounted on the three-axis stabilized POES spacecraft so that the centre of each detector field of view is outward along the local zenith, parallel to the Earth-centre-to-satellite radial vector. Another set of detectors, termed the 90º-detectors are mounted approximately perpendicular to the 0° detector. In addition, there is also a set of omnidirectional measurements made from a dome detector which is mounted parallel to the 0º detectors. The detectors pointing in the 0º and 90º directions are ±15º wide, while the omindirectional dome detectors (termed "omni") are ±60º wide. For the *L*-shells we consider the 90º-detector appears to primarily respond to trapped electrons, and hence we will refer to it as the "trapped detector". In Figure 3 we show the >300 keV 90º POES trapped electron fluxes during the study period from May to November 2007, indicating the influence of HSSWS (solar wind speed is shown by the white line in the small upper panel) on the energetic electron fluxes in the outer radiation belt. The black shading indicates a lack of data.

Ground-based magnetometer data are also analyzed in this study, particularly for ULF phenomena in the higher part of this frequency band (i.e., up to 5 Hz). The

locations of the magnetometers at Lucky Lake (LCL) and Island Lake (ISLL) are shown in Figure 2. The Island Lake magnetometer is part of the CARISMA network [Mann et al., 2008]. The Narod fluxgate magnetometers there provide a data stream sampled at 8 Hz. At Lucky Lake a search coil magnetometer data is sampled at 10 Hz, and is operated by the University of Tokyo. We determine the daily average ULF intensity having filtered over the bandwidth of interest. In the Pc4-5 range we used 1-22 mHz from the Island Lake magnetometer, and in the Pc1-2 range we used 0.1-5 Hz from the Lucky Lake magnetometer during the study period in 2007.

3. Results

3.1 Energetic electron precipitation

As mentioned above, when energetic electron precipitation ionizes the atmosphere it typically changes the propagation conditions for transmitter signals by modifying the upper boundary condition of the subionospheric waveguide. The lower boundary, being the land or sea surface, is regarded as remaining constant with time. Under non-disturbed ionospheric conditions the upper boundary conditions of the subionospheric waveguide will vary throughout the day as the Sun rises and sets. Typically we would expect to observe higher amplitude transmitter signals during the night, and lower amplitudes during the day, with deep minima during the sunrise and sunset periods [e.g., Clilverd et al., 1999].

In Figure 4 we show the typical diurnal variations of the amplitude of the three transmitters, NAA, NDK, and NLK, received at Churchill during several phases of a geomagnetic storm which occurred on 22-25 May 2007. In each panel there are three

lines representing: a non-disturbed pre-storm variation (solid line); an initial storm phase variation (dotted line); and a main storm phase variation (dashed line). The pre-storm data shown is from either 18th or 21st May 2007. The selection is primarily influenced by the need for the transmitter to be transmitting for the whole of the day, and not under going any off-air maintenance. The initial storm data is taken from either 23rd or 24th May 2007, and the main phase data taken from 26th May 2007. The storm-time variations from all three transmitters follow basically the same pattern, i.e., during a geomagnetic storm the nighttime amplitude decreases, and the daytime amplitude increases relative to the non-disturbed behaviour. This is consistent with increased ionization at altitudes that define the upper boundary for subionospheric propagation of ~25 kHz radio waves, i.e., below ~85 km during the night and below ~72 km during the day [McRae and Thomson, 2000; Thomson and Clilverd, 2007]. This suggests an experimental sensitivity to electron precipitation energies >50 keV at night and >200 keV during the day [Turunen et al., 2009]. In the following figures we determine the difference in amplitude between the daytime average and the nighttime average (Amp diff). During non-disturbed periods nighttime amplitudes are higher than daytime, and thus the difference is negative. During disturbed periods the difference becomes more positive as the nighttime amplitudes become lower than the daytime ones. This behaviour has been observed previously as a result of enhanced ionisation events such as solar proton events [Clilverd et al., 2006b], has been modelled successfully in terms of general ionisation enhancements [Clilverd et al., 2007], and has been used to study changes of ionisation for observation periods of many months [Clilverd et al., 2009]. The phases

of the transmitter signals also show distinct changes as a result of electron precipitation with the most significant change being observed as a phase advance during the nighttime. However in this paper we confine ourselves to discussing amplitude changes as they are more readily analysed over the multi-month period analysed in this paper, and consistent with previous analysis of this type [Clilverd et al., 2007].

3.2 Comparison with ΣKp

Figure 5 shows the day-night amplitude difference (diamonds) for the three transmitters from 19 May-05 November 2007. The data stopped on 05 November (day 308) due to a long-term system fault at Churchill. The panels are arranged to represent the average longitude of the transmitter-receiver paths ordered with the eastern-most in the top panel, i.e., NAA. Also plotted in each panel is the 7-day smoothed daily sum Kp (solid line) scaled to fit the difference amplitude variations, and the vertical dot-dashed lines as shown in Figure 1 to represent the peaks of the recurrent storm activity cycles 1, 2, 3, and 4. The lower panel shows the average daytime riometer absorption from Gillam (L=6.3) which is located in central Canada and should be representative of electron precipitation from the outer radiation belts in the energy range 30-200 keV [Little and Lienbach, 1959; Browne et al., 1995].

This Figure shows that as the geomagnetic activity varies so does the amplitude difference for each transmitter, indicating the presence of varying energetic electron precipitation as a result of enhanced geomagnetic activity. Following the large storm towards the end of May 2007 (day ~147, shown in Figure 4) a period of relatively

quiet geomagnetic activity occurred until the onset of the recurrent activity starting day ~210. During the four cycles of the recurrent activity for which we have data the amplitude difference shows a consistent positive response to the increased geomagnetic activity, only returning to normal levels in between the cycle peaks. However, particularly following the most intense geomagnetic activity periods (cycles 2 and 3; days ~250 and ~280), the amplitude differences remain high for ~10-15 days afterwards, despite the fact that geomagnetic activity has subsided to lower levels, particularly for Kp. This is true for the observation paths sampled by all three transmitters. The lower panel in Figure 5 shows that the riometer response does not behave in a similar way, peaking in absorption briefly, and apparently responding only during the time of the peak of the geomagnetic activity. This therefore suggests that the energy of the electron precipitation driving the elevated VLF radio wave amplitude difference response is >200 keV, and thus would not be registered by the riometer.

3.3 Comparison with Dst

Although Kp is a well known geomagnetic activity index we can also compare the amplitude difference variations with another index of geomagnetic disturbance, Dst. Dst is calculated from the average value of the horizontal component of the geomagnetic field measured at four near-equatorial geomagnetic observatories, and is a measure of the energy density of the ring current. Typically Dst shows a negative deviation during geomagnetic storms. Recurrent geomagnetic storms typically show Dst values of ~-50 nT [Borovsky and Denton, 2006]. In Figure 6 we show the

amplitude difference data for each of the three transmitters, and the riometer absorption from Gillam in the same format as Figure 5. However for this figure we include the smoothed daily Dst variation scaled to fit the amplitude data. In order to do this we invert the Dst scale. The figure shows that Dst can be a good indicator of the recurrent storm effects on the amplitude difference data. By comparison with Figure 5 it is clear that the Dst index captures the onset of the storm effect more accurately than Kp. This particularly noticeable for the storm in May 2007 (day ~147), and recurrent storm cycle 3. Dst is also more accurate in representing the decline in the recurrent storm effect than Kp, although the NAA transmitter in particular still shows some elevated amplitude difference values after Dst has returned to non-storm levels.

The lower panel in Figure 6 shows that the riometer response does not match the variation in Dst particularly closely. In much the same way as with Kp, the riometer absorption only shows any significant response at the approximate times of the peaks in Dst activity.

3.4 Comparison with satellite data

Since the VLF radio waves from NAA, NDK, and NLK propagate beneath the region of the sub-ionospheric waveguide that is influenced by electron precipitation from the outer radiation belt we compare the amplitude difference variations with the average $3<L<7$ electron flux variations observed from POES. Figure 7 shows the amplitude difference for each transmitter (diamonds joined by a dotted line) and the $3<L<7$ average POES 90° >300 keV trapped fluxes (solid line). As in previous

figures the recurrent cycles in geomagnetic activity are labelled by 1, 2, 3, and 4, with the timing of the peak taken from Figure 1 and indicated by vertical dot-dashed lines. From this Figure we can see that the behaviour of the amplitude difference from each transmitter is well represented by the variations in the >300 keV fluxes. This is particularly true for cycles 1 and 2, but not for the latter half of cycle 3 where there are enhanced amplitude differences even after the >300 keV electron fluxes have returned to near-zero levels, particularly around day 285. As this is not observed in the riometer data (shown in Figures 5 and 6) or the >300 keV fluxes we investigate the possibility that there is even more energetic electron precipitation, at energies significantly beyond 300 keV, i.e., around 1 MeV, happening during this period, which is not correlated with lower energy >300 keV precipitation.

As there is a large component of the difference amplitudes that is well-described by the >300 keV fluxes we can remove that effect by scaling the fluxes as shown in Figure 7, and then subtracting them from the difference values. The result is shown in Figure 8. The diamonds represent the remnant amplitude difference values during the study period, while each panel shows one of the three transmitters. Once again, we look for consistency between the three transmitter datasets to confirm that we are not just seeing noise. In each panel we also plot the POES ~1 MeV onmi detector trapped flux (solid line) averaged from $3<L<7$. The 1 MeV electron fluxes are measured as a contaminant of the 16 MeV proton dome onmi detector but, as there were no solar proton events during our study period, we can be confident that the fluxes are due to primarily trapped energetic electrons [Rodger et al., 2010]. The Figure shows that the remnant amplitude differences vary in a similar way to the

~1 MeV electron fluxes for all three transmitters, particularly ~10-15 days after recurrent activity cycle 3. Thus it appears most likely that the long-lived VLF amplitude disturbance seen in our observations is due to a combination of >300 keV and relativistic (~1 MeV) electron precipitation, with a spectrum that hardens with time such that there is an increasing fraction of relativistic electrons.

Following the approach of Rodger et al. [Figure 8, 2010], who saw energy dependant time delays ranging from 1-12 days in the POES energetic electron data after recurrent storms, we consider the possibility that the enhanced difference amplitudes observed on all three transmitters after cycle 3 could be due to a delayed enhancement of high energy electron fluxes relative to lower energy electrons. In Figure 9, upper panel, we plot the day-night amplitude difference for the NAA transmitter (dotted line, open diamonds) and compare them with the results of adding together the equivalent amplitude effect of the POES >300 keV trapped electron flux determined from Figure 7 and the ~1 MeV trapped electron flux determined from Figure 8 (solid line, solid diamonds). The combination of the equivalent amplitude effect of the two energy ranges provides a reasonable description of the amplitude difference data in the top panel. In the middle panel we show the smoothed daily sum Kp (solid line) with the >300 keV fluxes shifted earlier by 4 days, and the ~1 MeV fluxes shifted earlier by 12 days. The smoothed daily sum Kp (solid line) is not shifted in time at all. A very clear phasing of several recurrent activity cycles can be seen suggesting that there is an increased delay for increasing electron energies, which is the same as the results of Rodger et al. [2010] who attributed this delay to the effects of wave-particle interaction processes taking place in the outer radiation

belt following recurrent geomagnetic activity. In the lower panel we show the smoothed daily Dst (solid line) with the >300 keV fluxes shifted earlier by 0 days, and the ~1 MeV fluxes shifted earlier by 9 days. This panel suggests that Dst is a good representation of the amplitude difference effects on NAA as represented by the POES >300 keV trapped electron flux, requiring 0 days offset. But a 9 day offset to the ~1 MeV fluxes is required to capture the full amplitude difference variation represented by the combination of >300 keV fluxes and ~1 MeV fluxes.

3.5 Comparison with ULF power variations

Mathie and Mann [2000] demonstrated that MeV electron flux enhancements at geostationary orbit (L=6.6) followed days of elevated Pc5 ULF wave power in the outer magnetosphere, suggesting that Pc5 pulsations were involved in the acceleration of electrons to MeV energies. An association between solar wind speed and Pc5 ULF wave power was shown for the first half of 1995, particularly involving recurrent fast solar wind speed streams. In this study Figure 1 shows that our study period involves recurrent high speed solar wind streams that have associated enhancements in geostationary MeV electron fluxes, suggesting the presence of enhanced ULF wave power. Further, Rodger et al. [2008] showed that the precipitation of ~1 MeV electrons into the atmosphere at L~4-5 was associated with electromagnetic ion-cyclotron waves (EMIC) observed in the ULF Pc1-2 range during periods of moderate geomagnetic activity. Summers and Thorne [2003] examined the mechanism of electron pitch-angle diffusion by gyroresonant interaction with EMIC waves as a cause of relativistic electron precipitation loss

from the outer radiation belt. They concluded that electrons with energy ≥1 MeV can be removed from the outer radiation belt by EMIC wave scattering during a magnetic storm over a time-scale of several hours to a day. Therefore we investigate the variation of Pc4-5 and Pc1-2 wave power observed at magnetometer sites that are located in Canada, and in the *L*-shell range between those of the VLF transmitters and the Churchill receiver. The time variations of the Pc4-5 and Pc1-2 wave power may allow us to infer some causative linkage to the delayed electron precipitation effects that are shown by the VLF radio wave data in Figure 5.

Figure 10 shows the daily average ULF intensity in the Pc4-5 range (1-22 mHz) from the Island Lake fluxgate magnetometer (ISLL, *L*=5.2), and ULF intensity in the Pc1-2 range (0.1-5 Hz) from the Lucky Lake search coil magnetometer (LCL, *L*=3.9, 10 Hz) during the study period in 2007. In the plot the y-axis units for ISLL and LCL are arbitrary and different, and cannot be compared. These magnetometer sites are marked as squares in Figure 2. Also shown in Figure 10 are the daily ΣKp and daily Dst variations and vertical lines to indicate the peak of the recurrent solar wind cycles. The variation of the Pc4-5 wave intensity (a proxy for power) was closely associated with the variation of ΣKp, and which we have shown in Figure 1 to be phase-locked to the solar wind speed. These observations of Pc4-5 wave intensity are consistent with the results of Mathie and Mann [2000]. The Pc4-5 intensity was not enhanced during days 280-285 when the VLF signals suggest the occurrence of electron precipitation. The variation of the Pc1-2 wave intensity is not as clearly associated with the ΣKp variation, but does show enhanced levels during days 280-285 consistent with the subionospheric VLF data.

The interpretation of Figure 10 suggests that while Pc4-5 wave power is enhanced at the same time as the solar wind speed and ΣKp it does not appear to play any role in the delayed electron precipitation that is observed with the VLF data. The association of high Pc4-5 wave power with high levels of geostationary MeV electron fluxes is consistent with the conclusion of Mathie and Mann [2000] in terms of the ULF waves accelerating electrons to high energy in the magnetosphere. Conversely the period of enhanced Pc1-2 wave intensity is consistent with the electron precipitation observed with the VLF data. This suggests that Pc1-2 wave power is involved in the electron loss processes from the magnetosphere, dumping them into the atmosphere. The location of the Lucky Lake magnetometer site, from which the Pc1-2 wave power was determined, is close to the outer edge of the plasmasphere (L~4), and so the electron precipitation may be associated with EMIC waves located near the plasmapause [Fraser and Nguyen, 2001]. Further work is required to accurately locate the region of electron precipitation, and model the VLF response to it. Although the energy of electron precipitation that has been associated with EMIC waves is ~1 MeV [Rodger et al., 2008], and we have shown in this study that enhanced fluxes of ~1 MeV electrons are also observed by the POES satellites, it is as yet unclear why the loss process takes place with such a delay compared with the geomagnetic storm and the associated electron acceleration processes.

5. Discussion and Summary

In 2007 we operated a radio receiver at Churchill, Canada from May-November. During that period the phase and amplitude from three U.S. ~25 kHz transmitters

were recorded (call-signs NAA, NDK, and NLK). Geomagnetic activity during the study period was generally low, as would be expected for the minimum of the 11-year solar activity cycle. However there were four cycles of recurrent geomagnetic activity spaced ~27 days apart generated by a co-rotating interaction region, with daily ΣKp reaching ~30 at the peaks of the disturbances, and daily Dst reaching ~-30 nT. The difference in the amplitude of the transmitters between daytime and nighttime varied with geomagnetic activity and was used as a proxy for subionospheric ionization changes caused by energetic electron precipitation during the geomagnetic storms. We used the day-night amplitude differences to investigate the variation of electron precipitation from the outer radiation belt during the recurrent geomagnetic storms.

For the most intense of the recurrent geomagnetic storms there was evidence of electron precipitation between L=3 and L=7 for 10-15 days after the peak of the disturbance as measured by sum Kp and daily Dst. The lesser disturbances showed precipitation effects that lasted for 5-10 days after the peak disturbance. This was found to be consistent with the time variation of the fluxes of >300 keV and ~1 MeV trapped electrons measured by POES. Using equivalent amplitude effects of the POES >300 keV and ~1 MeV trapped electron fluxes it was possible to explain the majority of the time variation of the difference amplitudes from all three transmitters during the recurrent storm activity. This suggests that the POES trapped fluxes in this energy range can be used as a reasonable proxy for the electron precipitation fluxes in the bounce loss-cone, which are much harder to measure, and subject to more influence of proton contamination [Rodger et al., 2010]. However we should note

that this conclusion has only been shown to hold for recurrent storm activity, and on a daily average basis. Other geomagnetic activity influences and in particular, shorter time-scales, may not show such a relationship. Further analysis of radio wave data from Churchill is planned to address this issue.

In combining the POES >300 keV and ~1 MeV trapped electron fluxes to reproduce the day-night amplitude difference variations observed, we determined that the recurrent storm activity acted on the different energies with different delay times. Relative to the smoothed daily ΣKp, the >300 keV electron fluxes peaked after a delay of 4 days, while the ~1 MeV electron fluxes peaked after a delay of 12 days. This is consistent with the findings of Roger et al. [2010] who found this type of increasingly delayed response with increasing electron energy in several periods of recurrent storm activity during the declining phase of solar cycle 23, typically averaging to 2 days delay for >300 keV and 8 days for ~1 MeV electrons. Relative to the smoothed daily Dst, the POES >300 keV electron fluxes peaked after a delay of 0 days, while the POES ~1 MeV electron fluxes peaked after a delay of 9 days, showing Dst to be a good measure of the effect of >300 keV electron fluxes.

The daily average ULF intensity over the Pc4-5 range from Island Lake (ISLL, L=5.2), and ULF intensity over the Pc1-2 range from Lucky Lake (LCL, L=3.9), both situated between the VLF transmitters and the Churchill receiver, show variations during the study period. The ULF Pc4-5 wave intensity was not elevated during the period during which ~1 MeV electron precipitation was identified, but varied in phase with the solar wind speed as with previous findings. The ULF Pc1-2 wave intensity was elevated during the ~1 MeV electron precipitation period following the

third and most intense of the recurrent geomagnetic activity cycles, and is consistent with a picture that involves Pc1-2 waves in radiation belt loss processes. The presence of time delays for higher energy electrons is consistent with a "cartoon" view of electron acceleration processes, for example through cyclotron interactions with whistler-mode waves, such that electrons are accelerated to progressively higher energies over time [Horne et al., 2005]. The precipitation of ~1 MeV electrons into the atmosphere appears to be more associated with the delayed appearance of a loss mechanism involving Pc1-2 waves (i.e., EMIC waves), than as a direct consequence of an ever present loss mechanism that is purely responding to the increase in high energy fluxes through electron acceleration. Clearly, both electron acceleration and loss processes need to be active in order to generate significant levels of energetic electron precipitation into the atmosphere, and further investigation beyond this event study are required to understand the detailed balance between these processes.

The importance of energetic electron precipitation into the atmosphere has been demonstrated by many authors [e.g., Rozanov et al., 2005; Seppälä et al., 2009]. A key mechanism is the production of chemicals at high latitudes during the polar winter which can catalytically destroy ozone and hence change the radiative balance of the atmosphere [Brasseur and Solomon, 2005]. In global climate models energetic electron precipitation must either be represented by measurements from the ground or spacecraft, or by a proxy such as Kp or Ap. In this study we have shown that for one type of geomagnetic activity (recurrent HSSWS) the >300 keV trapped electron flux from POES is a reasonable measurement to use, although it does not capture all of the variability of the electron precipitation from the outer radiation belt. We have

also shown that it may be possible to describe energetic electron precipitation using a proxy such as Kp or Dst, but that, particularly for Kp, careful incorporation of time delays for different electron energies must be considered. Further work is needed to determine the energetic electron precipitation fluxes and spectra that are suggested by the >300 keV trapped fluxes.

Acknowledgments. The authors would like to acknowledge the support and enthusiasm of LeeAnn Fishback and Carley Basler at the Churchill Northern Studies Centre, Churchill, Canada. MAC and TM-G would also like to acknowledge NERC funding as part of the Climate programme at the British Antarctic Survey. The magnetometer data from Lucky Lake was provided under the STEP Polar Network program (url: http://step-p.dyndns.org/~khay/). CARISMA is operated and deployed by the University of Alberta, funded by the Canadian Space Agency.

References

Barr, R., D. L. Jones, and C. J. Rodger (2000), ELF and VLF radio waves, J. Atmos. Sol.-Terr. Phys., 62, 1689-1718.

Blake, J. B., M. D. Looper, D. N. Baker, R. Nakamura, B. Klecker, and D. Hovestadt (1996), New high temporal and spatial resolution measurements by SAMPEX of the precipitation of relativistic electrons, Adv. Space Res., 18(8), 171–186.

Borovsky, J. E., and M. H. Denton (2006), Differences between CME-driven storms and CIR-driven storms, J. Geophys. Res., 111, A07S08, doi:10.1029/2005JA011447.

Brasseur, G., and S. Solomon (2005), *Aeronomy of the Middle Atmosphere*, third ed., D. Reidel Publishing Company, Dordrecht.

Browne, S., J. K. Hargreaves, and B Honary, (1995): An Imaging Riometer for Ionospheric Studies, Elect. Comm. Eng. J., 7, 209–217.

Clilverd, M A, N R Thomson, and C J Rodger (1999), Sunrise effects on VLF signals propagating over a long north-south path, Radio Sci., 34(4), 939-948.

Clilverd, M. A., C. J. Rodger, T. Ulich, A. Seppälä, E. Turunen, A. Botman, and N. R. Thomson (2005), Modeling a large solar proton event in the southern polar atmosphere, *J. Geophys. Res.*, 110, A09307, doi:10.1029/2004JA010922.

Clilverd, M. A., A. Seppälä, C. J. Rodger, N. R. Thomson, P. T. Verronen, E. Turunen, Th. Ulich, J. Lichtenberger, and P. Steinbach (2006a), Modeling polar ionospheric effects during the October-November 2003 solar proton events, Radio Sci., 41, RS2001, doi:10.1029/2005RS003290.

Clilverd, M. A., A. Seppälä C. J. Rodger, P. T. Verronen, and N. R. Thomson (2006b), Ionospheric evidence of thermosphere-to-stratosphere descent of polar NO_X, Geophys. Res. Lett., 33, L19811, doi:10.1029/2006GL026727.

Clilverd, M. A, A Seppälä, C J Rodger, N R Thomson, J Lichtenberger, and P Steinbach (2007), Temporal variability of the descent of high-altitude NOX, J. Geophys. Res., 112, A09307, doi:10.1029/2006JA012085.

Clilverd, M. A., C. J. Rodger, N. R. Thomson, J. B. Brundell, Th. Ulich, J. Lichtenberger, N. Cobbett, A. B. Collier, F. W. Menk, A. Seppälä, P. T. Verronen, and E. Turunen (2009), Remote sensing space weather events: the AARDDVARK network, Space Weather, 7, S04001, doi:10.1029/2008SW000412, 2009.

Evans, D. S., and M. S. Greer (2004), Polar Orbiting environmental satellite space environment monitor - 2 instrument descriptions and archive data documentation, NOAA technical Memorandum version 1.4, Space Environment Laboratory, Colorado.

Fei, Y., A. A. Chan, S. R. Elkington, and M. J. Wiltberger (2006), Radial diffusion and MHD particle simulations of relativistic electron transport by ULF waves in the September 1998 storm, J. Geophys. Res., 111, (A12209), doi:10.1029/2005JA011211.

Fraser, B. J., and T. S. Nguyen (2001), Is the plasmapause a preferred source region of electromagnetic ion cycltron waves in the magnetosphere? J. Atmos. Terr. Phys., 63, 1225-1247.

Hilmer, R. V., G. P. Ginet, and T. E. Cayton (2000), Enhancement of equatorial energetic electron fluxes near L=4.2 as a result of high speed solar wind streams, J. Geophys. Res., 105 (A10), 23311-23322.

Horne, R.B. (2002), The contribution of wave-particle interactions to electron loss and acceleration in the Earth's radiation belts during geomagnetic storms, in URSI Review of Radio Science 1999-2002, edited by W.R. Stone, pp. 801-828, Wiley.

Horne R. B., R. M. Thorne, S. A. Glauert, J. M. Albert, N. P. Meredith, R. R. Anderson (2005), Timescale for radiation belt electron acceleration by whistler mode chorus waves, J. Geophys. Res., 110, A03225, doi:10.1029/2004JA010811.

Imhof, W. L., R. M. Robinson, H. L. Collin, J. R. Wygant, and R. R. Anderson (1992), Simultaneous measurements of waves and precipitating electrons in the outer radiation belt, Geophys. Res. Lett., 19(24), 2437–2440.

Little, C.G. and H. Leinbach, (1959), The riometer: a device for the continuous measurements of ionospheric absorption, Proc. IRE, 37, 315-320.

Longden, N., M. H. Denton, and F. Honary (2008), Particle precipitation during ICME-driven and CIR-driven geomagnetic storms, J. Geophys. Res., *113*, A06205, doi:10.1029/2007JA012752.

Lorentzen, K., M. Looper, and J. Blake (2001), Relativistic Electron Microbursts during the GEM Storms, Geophys. Res. Lett., 28(13), 2573-2576.

Mann, I.R., D. K. Milling, I. J. Rae, L. G. Ozeke, A. Kale, Z. C. Kale, K. R. Murphy, A. Parent, M. Usanova, D. M. Pahud, E.-A. Lee, V. Amalraj, D. D. Wallis, V. Angelopoulos, K.-H. Glassmeier, C. T. Russell, H.-U. Auster, and H. J. Singer (2008), The Upgraded CARISMA Magnetometer Array in the THEMIS Era, Space Sci. Rev., doi:10.1007/s11214-008-9457-6.

Manney, G. L., K. Kruger, J. L. Sabutis, S. A. Sena, and S. Pawson (2005), The remarkable 2003-2004 winter and other recent warm winters in the Arctic stratosphere since the late 1990s, J. Geophys. Res., 110, D04107, doi: 10.1029/2004JD005367.

Mathie, R. A., and I. R. Mann (2000), A correlation between extended intervals of ULF wave power and storm-time geosynchronous relativistic electron flux enhancements, Geophys. Res. Lett., 27, 3261-3264.

McRae, W M, and N R Thomson (2000), VLF phase and amplitude: daytime ionospheric parameters, J. Atmos. Sol.-Terr. Phys., 62(7), 609-618.

Millan, R. M., R. P. Lin, D. M. Smith, K. R. Lorentzen, and M. P. McCarthy (2002), X-ray observations of MeV electron precipitation with a balloon-borne germanium spectrometer, Geophys. Res. Lett., 29(24), 2194, doi:10.1029/2002GL015922.

Miyoshi, Y., and R. Kataoka (2005), Ring current ions and radiation belt electrons during geomagnetic storms driven by coronal mass ejections and corotating interaction regions, Geophys. Res. Lett., 32, L21105, doi:10.1029/2005GL024590.

O'Brien, T. P., M. D. Looper, and J. B. Blake (2004), Quantification of relativistic electron microburst losses during the GEM storms, Geophys. Res. Lett., 31, L04802, doi:10.1029/2003GL018621.

Omura, Y., Y. Katoh, and D. Summers (2008), Theory and simulation of the generation of whistler-mode chorus, J. Geophys. Res., *113*, A04223, doi:10.1029/2007JA012622.

Randall, C. E., et al. (2005), Stratospheric effects of energetic particle precipitation in 2003-2004, Geophys. Res. Lett., 32, L05802, doi:10.1029/2004GL022003.

Richardson, I. G., E. W. Cliver, and H. V. Cane (2000), Sources of geomagnetic activity over the solar cycle: Relative importance of coronal mass ejections, high-speed streams, and slow solar wind. J. Geophys. Res., 105 (A8), 18203-18213.

Rodger, C. J., M. A. Clilverd, P. T. Verronen, Th. Ulich, M. J. Jarvis, and E. Turunen (2006), Dynamic geomagnetic rigidity cutoff variations during a solar proton event, J. Geophys. Res., 111, A04222, doi:10.1029/2005JA011395.

Rodger, C. J., M. A. Clilverd, N. R. Thomson, R. J. Gamble, A. Seppälä E. Turunen, N. P. Meredith, M. Parrot, J. A. Sauvaud, and J.-J. Berthelier (2007), Radiation belt electron precipitation into the atmosphere: recovery from a geomagnetic storm, J. Geophys. Res., 112, A11307, doi:10.1029/2007JA012383.

Rodger, C. J., T. Raita, M. A. Clilverd, A. Seppälä S. Dietrich, N. R. Thomson, and Th. Ulich (2008), Observations of relativistic electron precipitation from the radiation belts driven by EMIC Waves, Geophys. Res. Lett., 35, L16106, doi:10.1029/2008GL034804.

Rodger, C. J., M. A. Clilverd, J. Green, and M.-M. Lam (2010), Use of POES SEM-2 observations to examine radiation belt dynamics and energetic electron precipitation in to the atmosphere, J. Geophys. Res., doi:10.1029/ 2008JA014023, (paper in press).

Rozanov, E., L. Callis, M. Schlesinger, F. Yang, N. Andronova, and V. Zubov (2005), Atmospheric response to NOy source due to energetic electron precipitation, Geophys. Res. Lett., 32, L14811, doi:10.1029/2005GL023041.

Seppälä, A., P. T. Verronen, E. Kyrölä, S. Hassinen, L. Backman, A. Hauchecorne, J. L. Bertaux, and D. Fussen (2004), Solar Proton Events of October-November 2003: Ozone depletion in the Northern hemisphere polar winter as seen by GOMOS/Envisat, Geophys. Res. Lett., 31(19), L19,107, doi:10.1029/2004GL021042.

Seppälä A., M. A. Clilverd, C. J. Rodger, P. T. Verronen, E. Turunen (2008), The effects of hard-spectra solar proton events on the middle atmosphere, J. Geophys. Res., 113, A11311, doi:10.1029/2008JA013517.

Seppälä, A., C. E. Randall, M. A. Clilverd, E. Rozanov, V. L. Harvey, and C. J. Rodger (2009), Geomagnetic activity and polar surface air temperature variability**,** *J. Geophys. Res.,* 114, A10312, doi:10.1029/2008JA014029.

Shea, M. A., and D. F. Smart (1990), A summary of major solar proton events, Solar Phys., 127(2), 297-320.

Siskind, D. E. (2000), On the coupling between the middle and upper atmospheric odd nitrogen, in Atmospheric science across the stratopause, Geophysical Mongraph 123, 101-116.

Solomon S, G. C. Reid, R. G. Roble, and P. J. Crutzen (1982), Photochemical coupling between the thermosphere and the lower atmosphere. I - Odd nitrogen from 50 to 120 km, J. Geophys. Res., 87, 7206-7220.

Spanswick, E., E. Donovan, and G. Baker (2005), Pc5 modulation of high energy electron precipitation: particle interaction regions and scattering efficiency, Ann. Geophys., 23, 1533-1542.

Summers, D., and R. M. Thorne (2003), Relativistic electron pitch-angle scattering by electromagnetic ion cyclotron waves during geomagnetic storms, J. Geophys. Res., *108*(A4), 1143, doi:10.1029/2002JA009489.

Summers, D., R. L. Mace, and M. A. Hellberg (2005), Pitch-angle scattering rates in planetary magnetospheres, J. Plasma Phys., 71(3), 237.

Summers, D., B. Ni, and N. P. Meredith (2007), Timescales for radiation belt electron acceleration and loss due to resonant wave-particle interactions: 2. Evaluation for VLF chorus, ELF hiss, and EMIC waves, J. Geophys. Res., 112, A04207, doi:10.1029/2006JA011993.

Thomson, N. R., M. A. Clilverd, and W. M. McRae (2007), Nighttime ionospheric D region parameters from VLF phase and amplitude, J. Geophys. Res., 112, A07304, doi:10.1029/2007JA012271.

Thorne, R. M., T. P. O'Brien, Y. Y. Shprits, D. Summers, and R. B. Horne (2005), Timescale for MeV electron microburst loss during geomagnetic storms, J. Geophys. Res., 110, A09202, doi:10.1029/2004JA010882.

Turunen, E., P. T. Verronen, A. Seppälä, C. J. Rodger, M. A. Clilverd, J. Tamminen, C. F. Enell and Th. Ulich (2009), Impact of different precipitation energies on NOx generation during geomagnetic storms, J. Atmos Sol.-Terr. Phys., 71, pp. 1176-1189, doi:10.1016/j.jastp.2008.07.005.

Vassiliadis, D., I. R. Mann, S. F. Fung, and X. Shao (2007), Ground Pc3-Pc5 wave power distribution and response to solar wind velocity variations, Planet. Space Sci., 55 (6), 743-754.

Verronen, P. T., A. Seppälä, M. A. Clilverd, C. J. Rodger, E. Kyrölä, C. Enell, T. Ulich, and E. Turunen (2005), Diurnal variation of ozone depletion during the October–November 2003 solar proton events, J. Geophys. Res., 110, A09S32, doi:10.1029/2004JA010932.

---

[1]M. A. Clilverd, T. Moffat-Griffin, P. Breen, British Antarctic Survey, High Cross, Madingley Road, Cambridge CB3 0ET, England, U.K. (email: macl@bas.ac.uk , tmof@bas.ac.uk , pbree@bas.ac.uk)

[2]C. J. Rodger, Department of Physics, University of Otago, P.O. Box 56, Dunedin, New Zealand. (email: crodger@physics.otago.ac.nz)

[3]E. Spanswick, Dept. of Physics and Astronomy, University of Calgary, 2500 University Drive, Calgary, Alberta, Canada T2N 1N4 (email: emma@phys.ucalgary.ca)

[4]F. W. Menk, R.S.Grew, School of Mathematical and Physical Sciences, University of Newcastle, Callaghan, N.S.W., 2308, Australia. (email: fred.menk@newcastle.edu.au , russell.grew@gmail.com)

[5]K. Hayashi, Department of Earth and Planetary Physics, University of Tokyo, Tokyo 113, Japan. (email: qyi05527@nifty.ne.jp)

[6]I. R. Mann, Department of Physics, University of Alberta, Edmonton, Alberta, T6G 2J1, Canada. (email: imann@phys.ualberta.ca)

(Received N x, 2009 N x 27, 2009

accepted N x, 2010)

Figures

Figure 1. Geomagnetic conditions over May-November 2007. The daily solar wind speed, daily sum Kp, daily Dst, and daily GOES >2 MeV electron flux are plotted in separate panels. Each panel also shows a 7-day smoothed line (solid line) for each parameter. A 27-day recurrent period of high solar wind, geomagnetic activity, and high electron fluxes is indicted by the dot-dashed vertical lines.

Figure 2. The location of subionospheric propagation paths in the northern hemisphere from VLF transmitters (circles) to the AARDDVARK receiver site at Churchill (diamond). *L*-Shell contours for *L*=3, 4 and 6 are shown. The location of the Gillam riometer, as well as the Lucky Lake and Island Lake magnetometers are also indicated (asterisk and squares respectively).

Figure 3. The >300 keV 90° POES trapped electron fluxes during the study period in 2007, showing the presence of recurrent HSSWS influence on the energetic electron fluxes in the outer radiation belt. The upper panel indicates the daily average solar wind speed. Black shading indicates a lack of data. The periods of recurrent geomagnetic activity identified in Figure 1 are indicated by the vertical dashed lines.

Figure 4. The typical diurnal variations of the amplitude of NAA, NDK, and NLK signals received at Churchill during several phases of a geomagnetic storm in May 2007. In each panel there are three lines representing: a non-disturbed pre-storm variation (18 or 21 May 2007, solid line); an initial storm phase variation (23 or 24 May 2007, dotted line); and a main storm phase variation (26 May 2007, dashed line). Local time for the mid-point of each of the paths is shown at the top of each panel.

Figure 5. The day-night amplitude difference (diamonds) for the three transmitters from May-November 2007. Also shown in each panel is the 7-day smoothed daily sum Kp (solid line) scaled to fit the difference amplitude variations, and the vertical dot-dashed lines as shown in Figure 1 to represent the peaks of the recurrent storm activity cycles 1, 2, 3, and 4. The lower panel shows the average daytime riometer absorption from Gillam (diamonds, L=6.3) which is located in central Canada (see Figure 2).

Figure 6. The day-night amplitude difference (diamonds) for the three transmitters from May-November 2007 in the same format as Figure 5. Also shown in each panel is the 7-day smoothed daily Dst (solid line) scaled to fit the difference amplitude variations.

Figure 7. The day-night amplitude difference for NAA, NDK, and NLK, received at Churchill in 2007 (diamonds joined by a dotted line) compared with the $3<L<7$ averaged POES >300 keV trapped electron flux for the same period (solid line). Recurrent solar activity cycles are labeled 1, 2, 3, and 4.

Figure 8. The remnant amplitude difference values (diamonds) during the study period, each panel represents one of the three transmitters. Also plotted is the POES ~1 MeV trapped flux from the omni detector (solid line) averaged from $3<L<7$. Recurrent solar activity cycles are labeled 1, 2, 3, and 4.

Figure 9. The upper panel compares the NAA day-night amplitude difference (dotted line, open diamonds) with the result of combining the equivalent POES >300 keV trapped electron flux determined from Figure 7 and the equivalent ~1 MeV trapped electron flux determined from Figure 8 (solid line, solid diamonds).

The middle panel shows the equivalent smoothed daily sum Kp (solid line) and the >300 keV fluxes (dotted line) shifted earlier by 4 days, and the ~1 MeV fluxes (solid line, diamonds) shifted earlier by 12 days. The lower panel shows the equivalent smoothed daily Dst (solid line) and the >300 keV fluxes (dotted line) shifted earlier by 0 days, and the ~1 MeV fluxes (solid line, diamonds) shifted earlier by 9 days.

Figure 10. Daily average ULF Pc4-5 and Pc1-2 power received at Island Lake (ISLL, L=5.2) and Lucky Lake (LCL, L=3.9) compared with the variation of geomagnetic activity ($\sum$Kp) and daily Dst. Periods of recurrent geomagnetic activity are indicated by the vertical dashed lines.

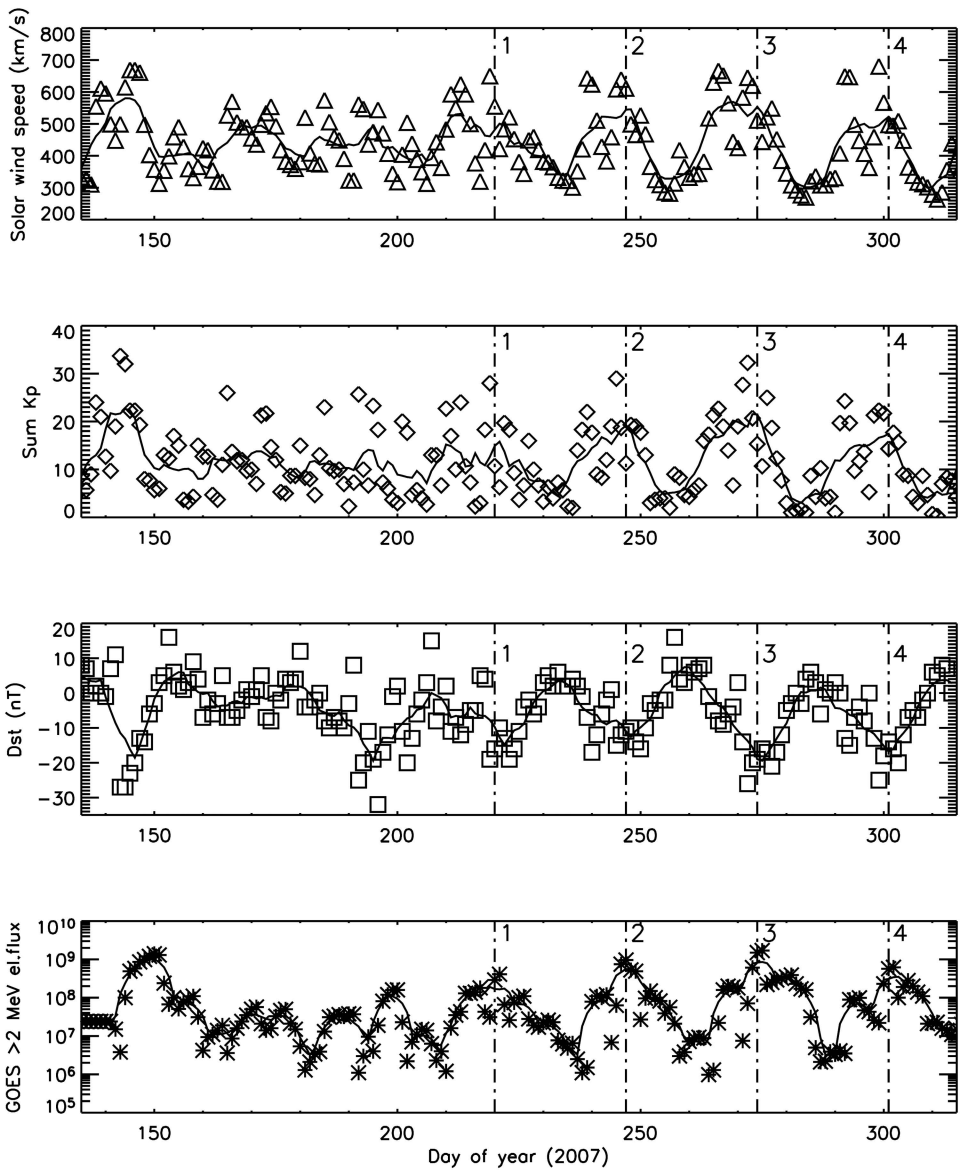
Solar wind speed (km/s)
800
700
600
500
400
300
200
1
2
3
4
150
200
250
300
Sum Kp
40
30
20
10
0
Dst (nT)
20
10
0
−10
−20
−30
GOES >2 MeV el.flux
10^{10}
10^{9}
10^{8}
10^{7}
10^{6}
10^{5}
Day of year (2007)

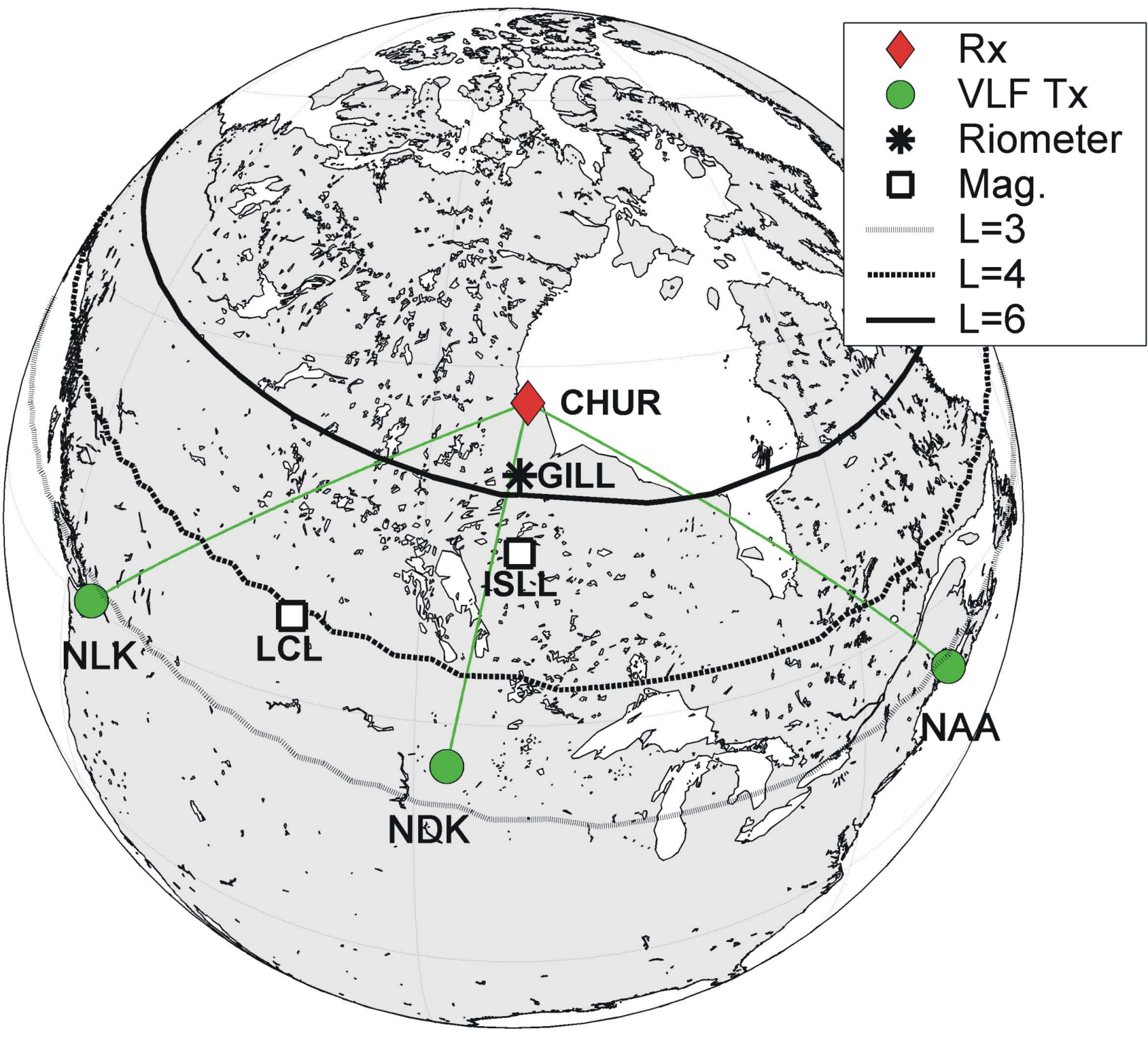
Rx
VLF Tx
Riometer
Mag.
L=3
L=4
L=6
CHUR
GILL
ISLL
LCL
NLK
NAA
NDK

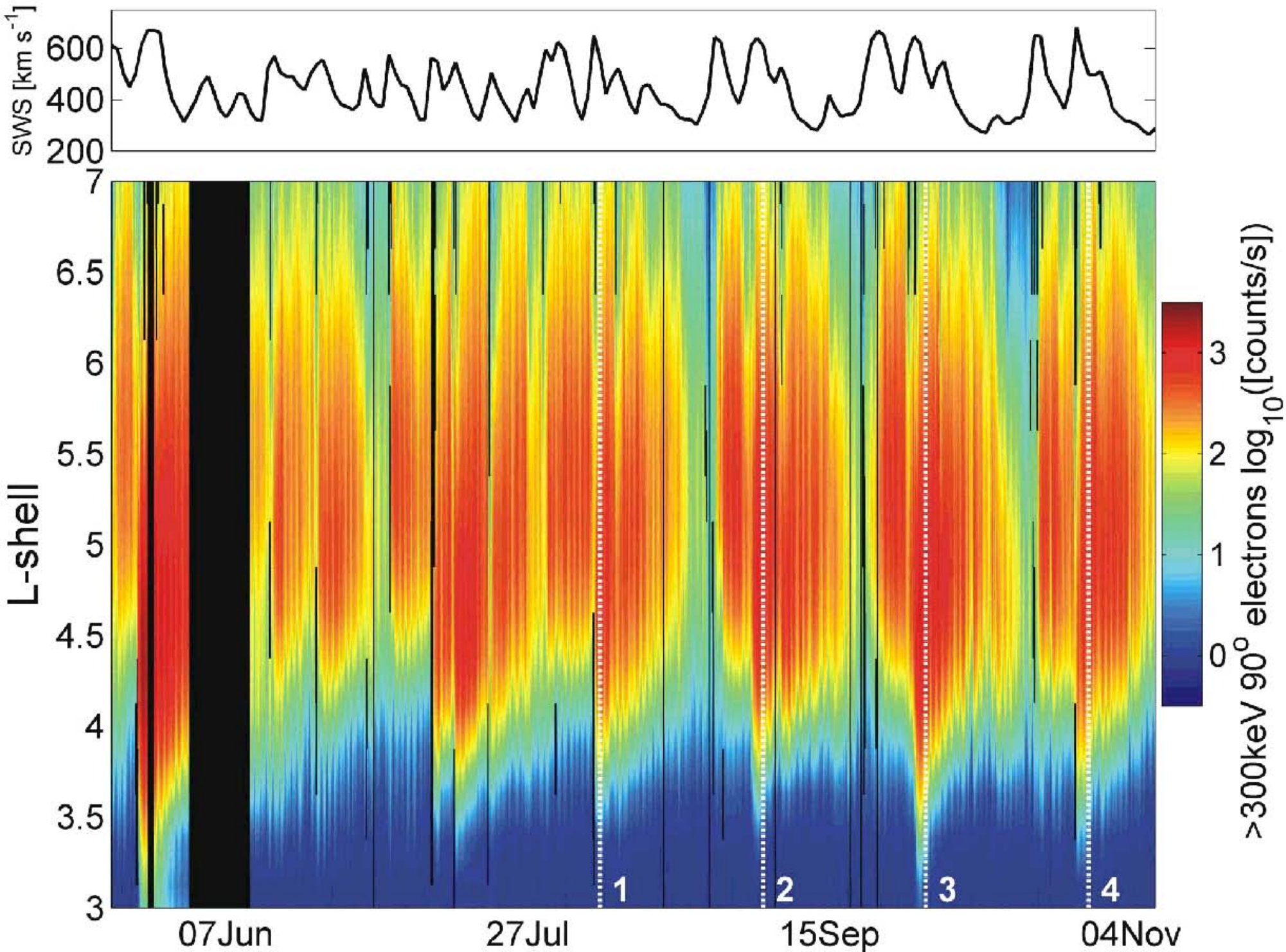
SWS [km s-1]
600
400
200
L-shell
7
6.5
6
5.5
5
4.5
4
3.5
3
1
2
3
4
07Jun
27Jul
15Sep
04Nov
>300keV 90° electrons log10([counts/s])
3
2
1
0

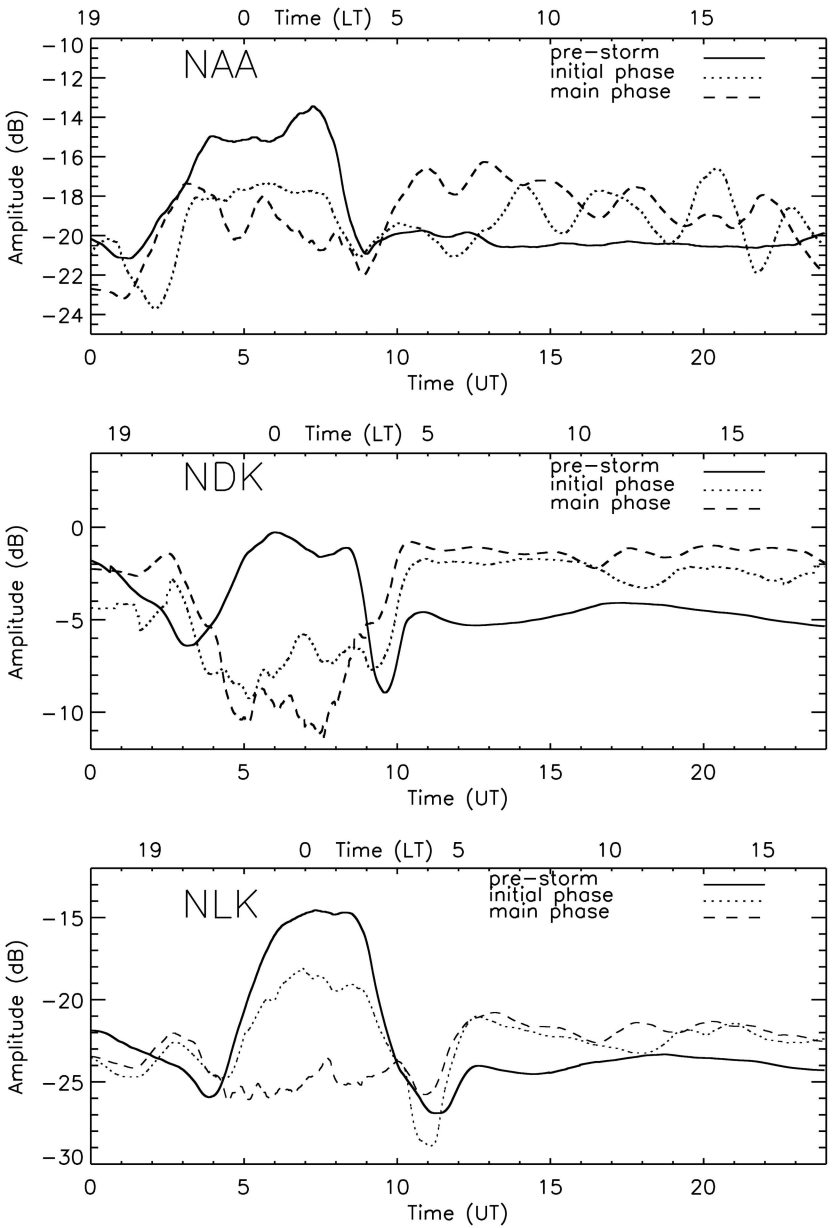
NAA
pre-storm
initial phase
main phase
19
0
Time (LT)
5
10
15
−10
−12
−14
−16
−18
−20
−22
−24
Amplitude (dB)
0
5
10
15
20
Time (UT)
NDK
pre-storm
initial phase
main phase
19
0
Time (LT)
5
10
15
0
−5
−10
Amplitude (dB)
0
5
10
15
20
Time (UT)
NLK
pre-storm
initial phase
main phase
19
0
Time (LT)
5
10
15
−15
−20
−25
−30
Amplitude (dB)
0
5
10
15
20
Time (UT)

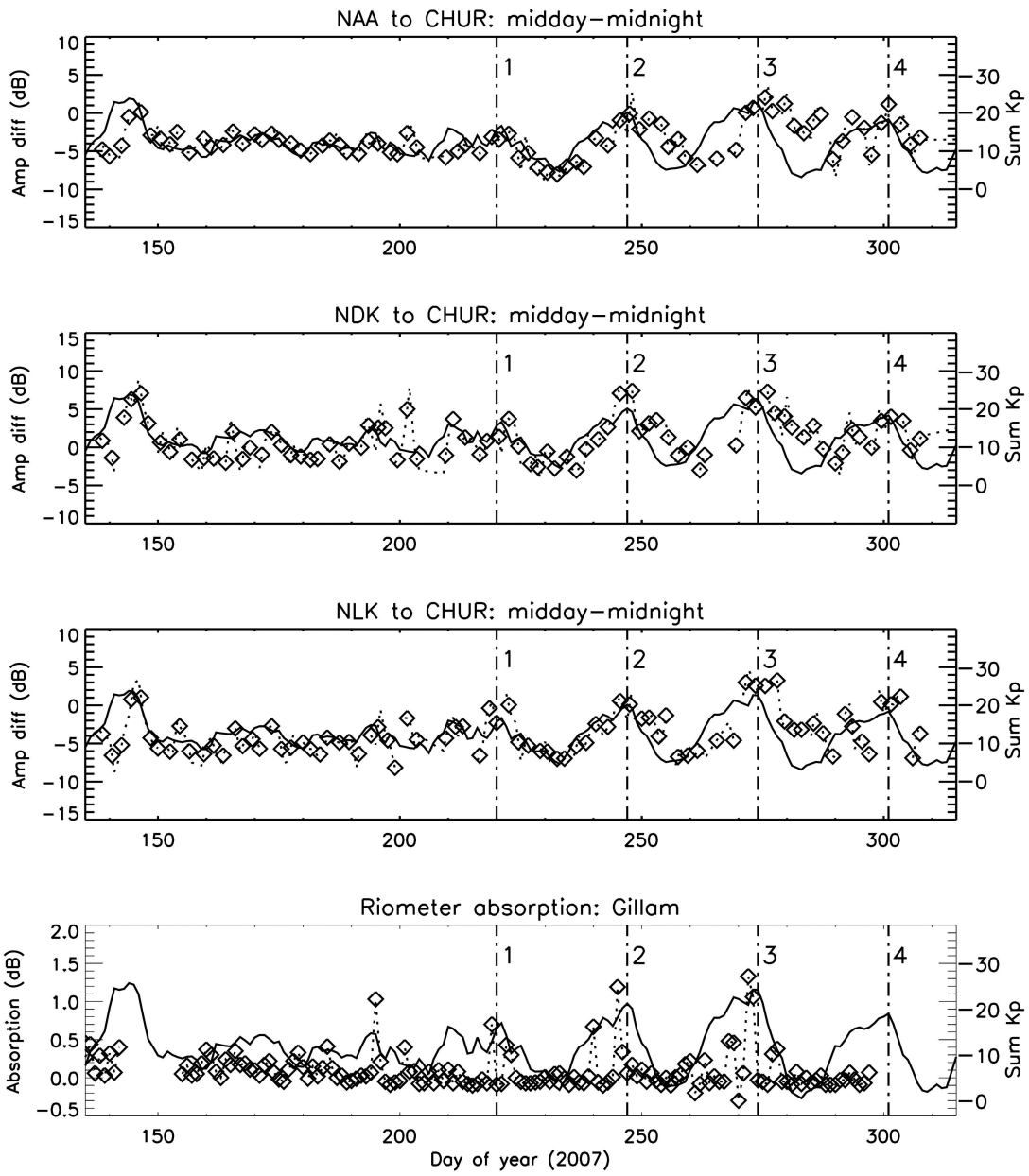
NAA to CHUR: midday−midnight
NDK to CHUR: midday−midnight
NLK to CHUR: midday−midnight
Riometer absorption: Gillam
Amp diff (dB)
Absorption (dB)
Sum Kp
1
2
3
4
150
200
250
300
Day of year (2007)

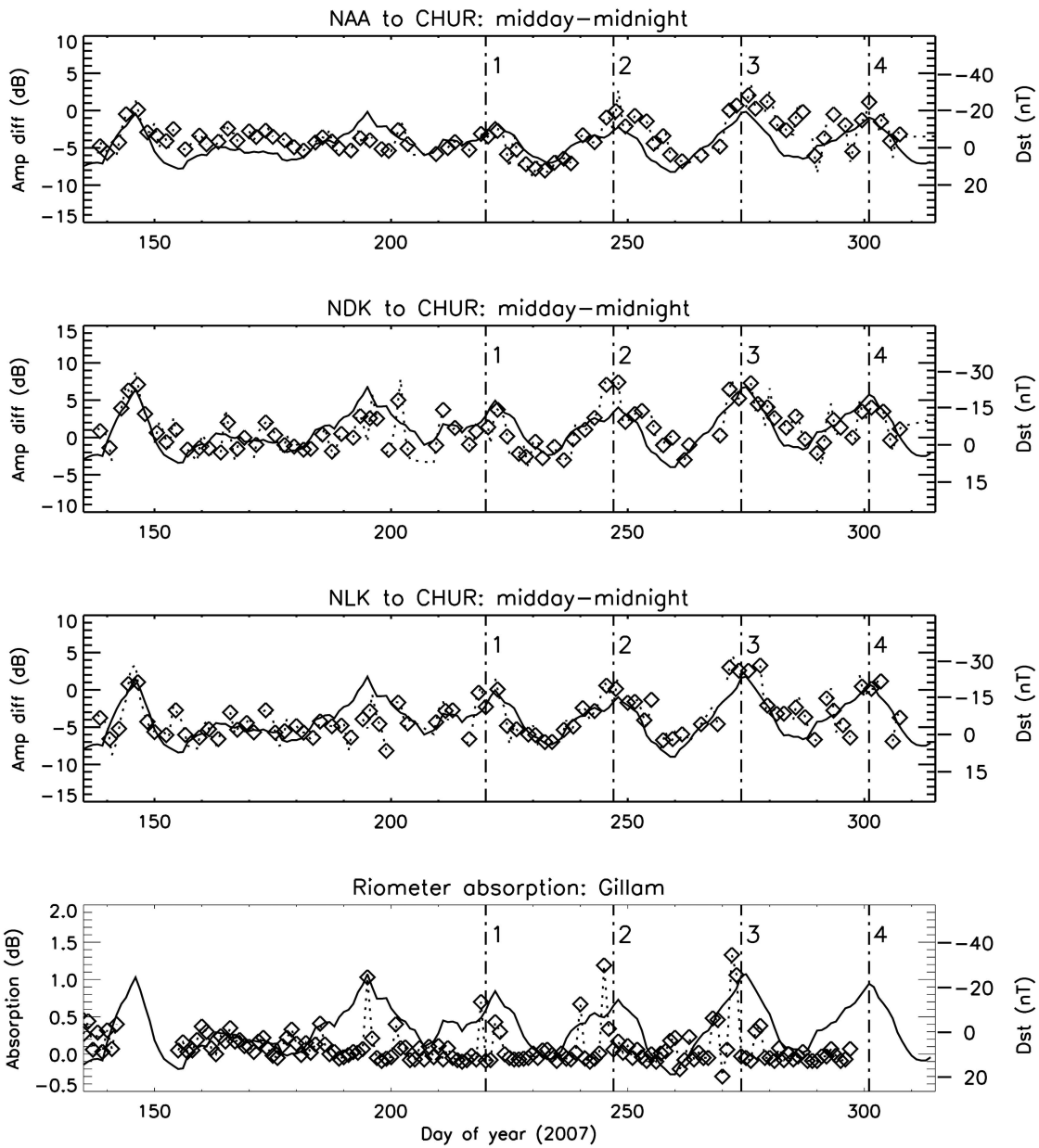
NAA to CHUR: midday−midnight
Amp diff (dB)
Dst (nT)
1
2
3
4
NDK to CHUR: midday−midnight
Amp diff (dB)
Dst (nT)
NLK to CHUR: midday−midnight
Amp diff (dB)
Dst (nT)
Riometer absorption: Gillam
Absorption (dB)
Dst (nT)
Day of year (2007)

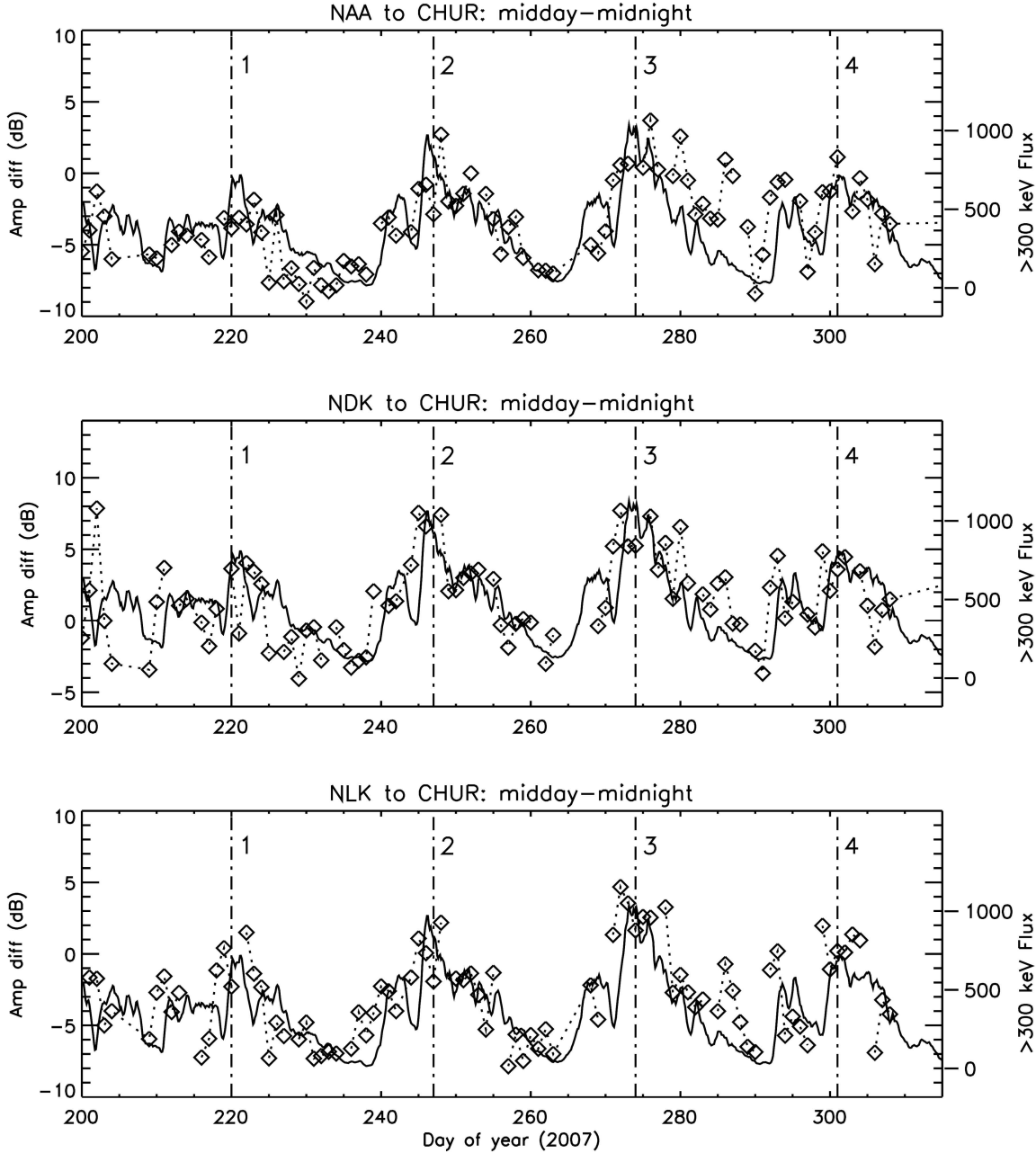
NAA to CHUR: midday−midnight
NDK to CHUR: midday−midnight
NLK to CHUR: midday−midnight
Amp diff (dB)
>300 keV Flux
Day of year (2007)
1
2
3
4
10
5
0
−5
−10
1000
500
0
200
220
240
260
280
300

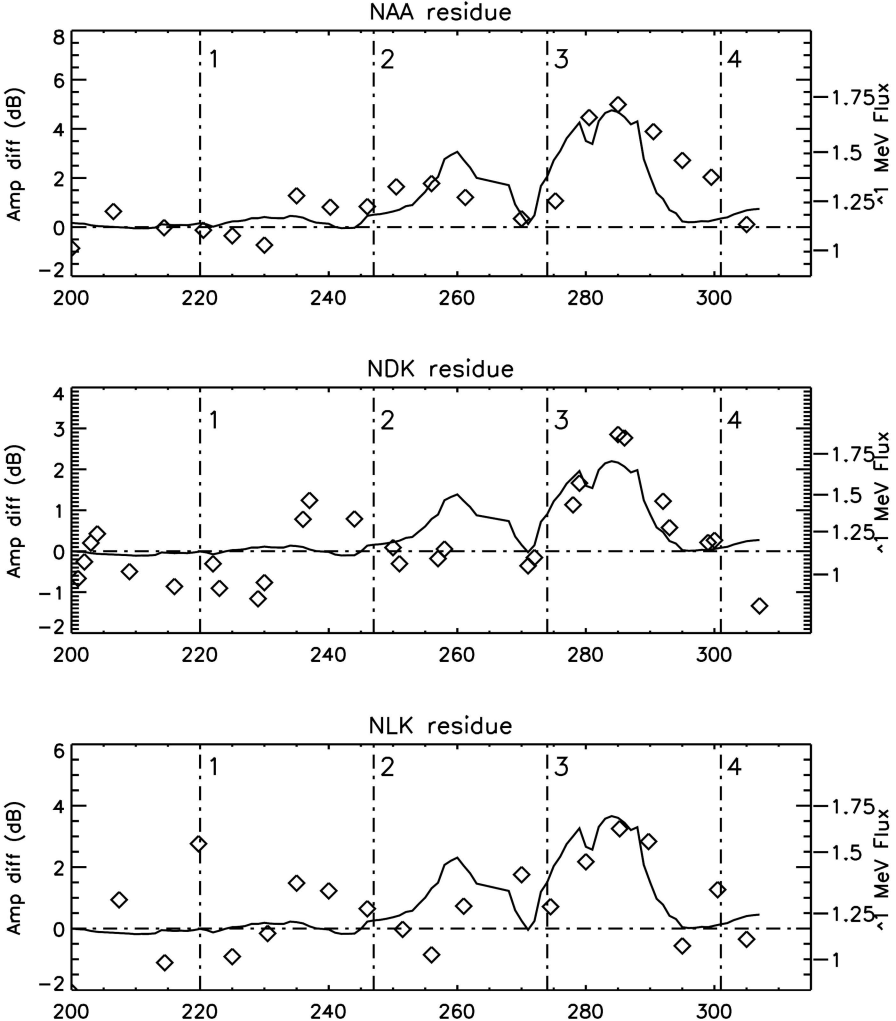
NAA residue
NDK residue
NLK residue
Amp diff (dB)
>1 MeV Flux
1
2
3
4
200
220
240
260
280
300

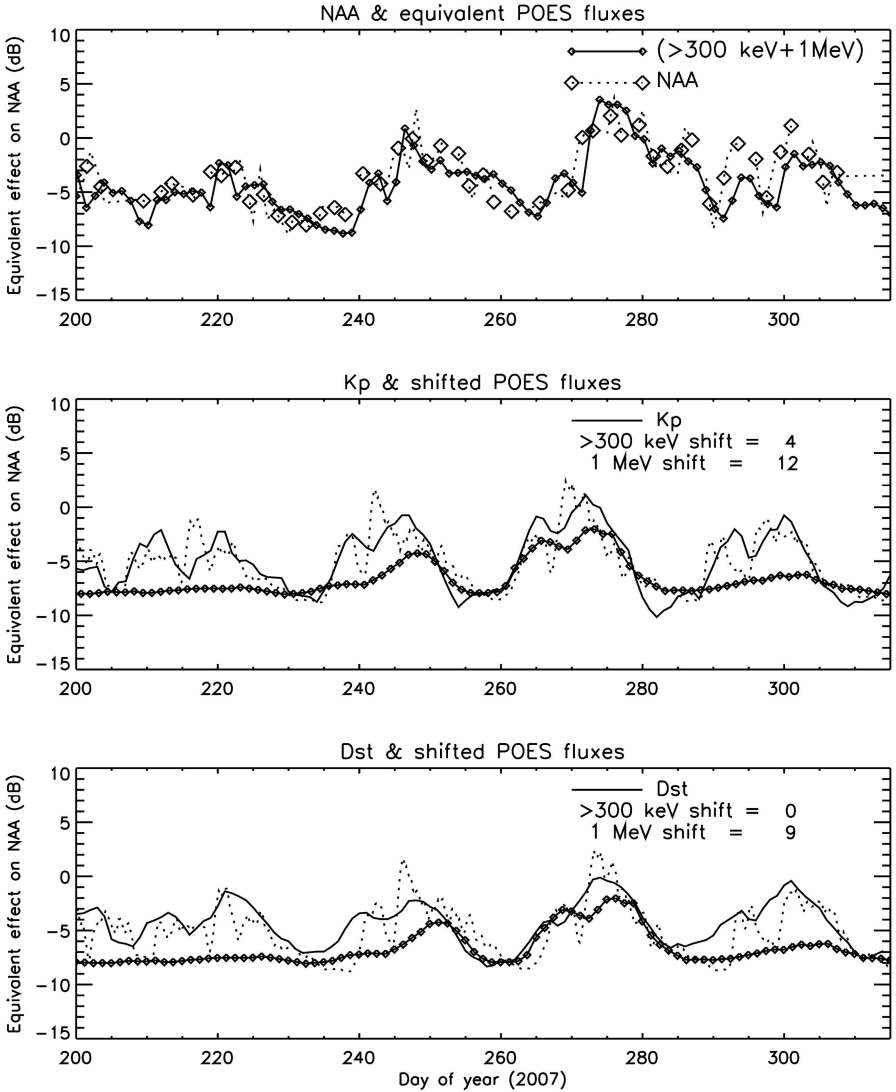
NAA & equivalent POES fluxes
(>300 keV+1MeV)
NAA
Equivalent effect on NAA (dB)
Kp & shifted POES fluxes
Kp
>300 keV shift = 4
1 MeV shift = 12
Dst & shifted POES fluxes
Dst
>300 keV shift = 0
1 MeV shift = 9
Day of year (2007)

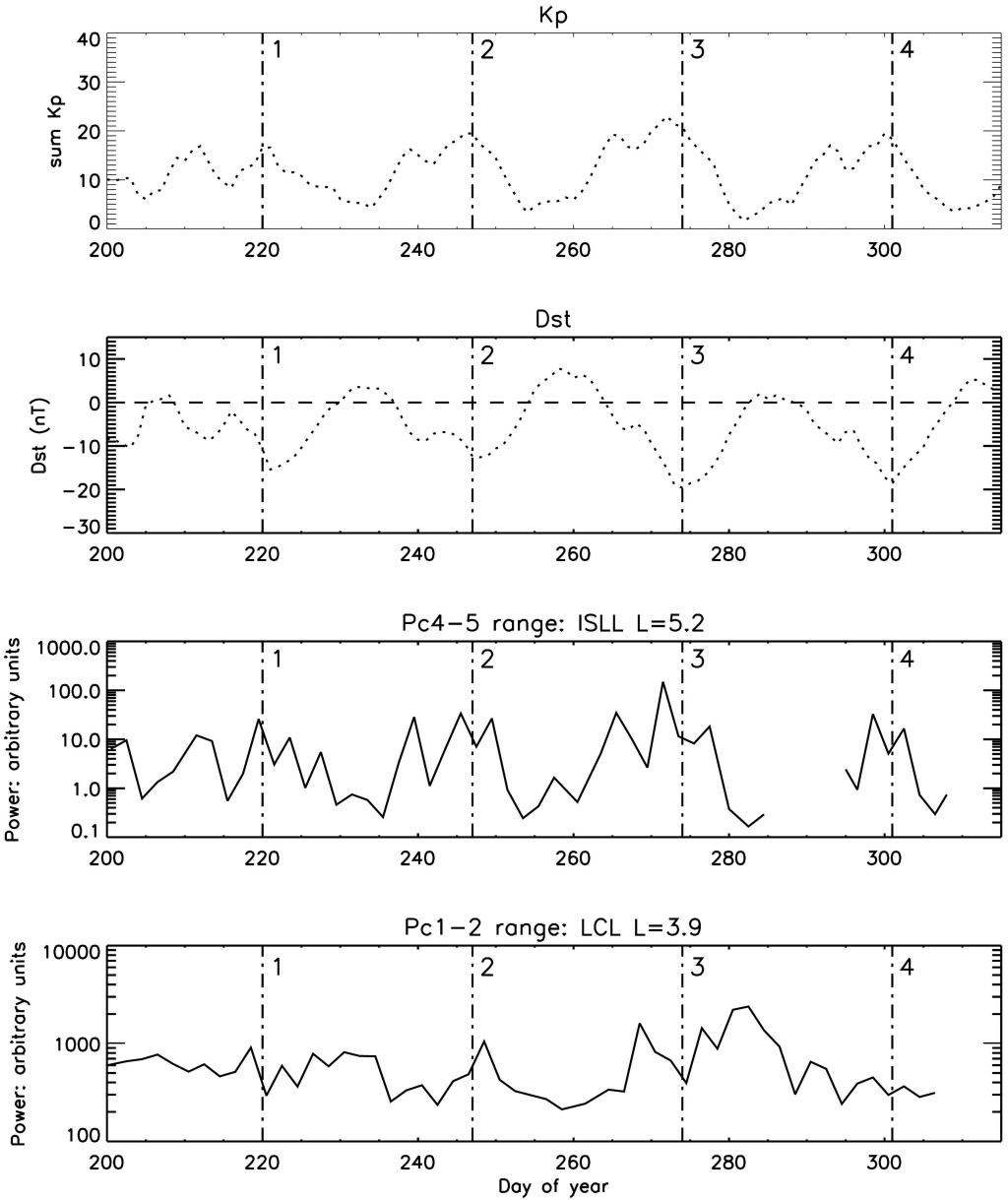
Kp
sum Kp
40
30
20
10
0
1
2
3
4
200
220
240
260
280
300
Dst
Dst (nT)
10
0
−10
−20
−30
Pc4−5 range: ISLL L=5.2
Power: arbitrary units
1000.0
100.0
10.0
1.0
0.1
Pc1−2 range: LCL L=3.9
10000
1000
100
Day of year